frontiers | Frontiers in Immunology

TYPE Original Research
PUBLISHED 17 May 2023
DOI 10.3389/fimmu.2023.1128239

OPEN ACCESS

EDITED BY
Diana Boraschi,
Shenzhen Institute of Advanced Technology (SIAT) (CAS), China

REVIEWED BY
Bernhard Ryffel,
Centre National de la Recherche Scientifique (CNRS), France
Piersante Sestini,
University of Siena, Italy

*CORRESPONDENCE
Carola Voss
carola.voss@helmholtz-muenchen.de
Anne Hilgendorff
anne.hilgendorff@med.uni-muenchen.de

RECEIVED 20 December 2022
ACCEPTED 23 March 2023
PUBLISHED 17 May 2023

CITATION
Kastlmeier MT, Gonzalez-Rodriguez E, Cabanis P, Guenther EM, König A-C, Han L, Hauck SM, See F, Asgharpour S, Bukas C, Burgstaller G, Piraud M, Lehmann M, Hatz RA, Behr J, Stoeger T, Hilgendorff A and Voss C (2023) Cytokine signaling converging on *IL11* in ILD fibroblasts provokes aberrant epithelial differentiation signatures. *Front. Immunol.* 14:1128239. doi: 10.3389/fimmu.2023.1128239

Cytokine signaling converging on *IL11* in ILD fibroblasts provokes aberrant epithelial differentiation signatures

Miriam T. Kastlmeier[1], Erika Gonzalez-Rodriguez[1], Phoebe Cabanis[1], Eva M. Guenther[1], Ann-Christine König[2], Lianyong Han[1], Stefanie M. Hauck[2], Fenja See[1], Sara Asgharpour[1], Christina Bukas[3], Gerald Burgstaller[1], Marie Piraud[3], Mareike Lehmann[1,4], Rudolf A. Hatz[5], Jürgen Behr[6], Tobias Stoeger[1], Anne Hilgendorff[1,7]* and Carola Voss[1]*

[1]Institute of Lung Health and Immunity, Helmholtz Center Munich, German Research Center for Environmental Health (GmbH), Comprehensive Pneumology Center Munich with the CPC-M bioArchive, Member of the German Center of Lung Research (DZL), Munich, Germany, [2]Metabolomics and Proteomics Core (MPC), Helmholtz Center Munich, German Research Center for Environmental Health (GmbH), Munich, Germany, [3]Helmholtz AI, Helmholtz Center Munich, German Research Center for Environmental Health (GmbH), Munich, Germany, [4]Institute for Lung Research, Philipps-University Marburg, Universities of Giessen and Marburg Lung Center, Member of the German Center for Lung Research (DZL), Marburg, Germany, [5]Klinik für Thoraxchirurgie, Asklepios Fachkliniken München-Gauting, Thoraxchirurgie, Munich, Germany, [6]Department of Medicine V, University Hospital, Ludwig-Maximilians University Munich, Comprehensive Pneumology Center, Member of the German Center for Lung Research (DZL), Munich, Germany, [7]Dr. von Haunersche Children's Hospital, Hospital of the Ludwig-Maximilians University, Member of the German Lung Research Center (DZL), Munich, Germany

Introduction: Interstitial lung disease (ILD) is a heterogenous group of lung disorders where destruction and incomplete regeneration of the lung parenchyma often results in persistent architectural distortion of the pulmonary scaffold. Continuous mesenchyme-centered, disease-relevant signaling likely initiates and perpetuates the fibrotic remodeling process, specifically targeting the epithelial cell compartment, thereby destroying the gas exchange area.

Methods: With the aim of identifying functional mediators of the lung mesenchymal-epithelial crosstalk with potential as new targets for therapeutic strategies, we developed a 3D organoid co-culture model based on human induced pluripotent stem cell-derived alveolar epithelial type 2 cells that form alveolar organoids in presence of lung fibroblasts from fibrotic-ILD patients, in our study referring to cases of pulmonary fibrosis, as well as control cell line (IMR-90).

Results: While organoid formation capacity and size was comparable in the presence of fibrotic-ILD or control lung fibroblasts, metabolic activity was significantly increased in fibrotic-ILD co-cultures. Alveolar organoids cultured with fibrotic-ILD fibroblasts further demonstrated reduced stem cell function as reflected by reduced Surfactant Protein C gene expression together with an aberrant basaloid-prone differentiation program indicated by elevated Cadherin

2, Bone Morphogenic Protein 4 and Vimentin transcription. To screen for key mediators of the misguided mesenchymal-to-epithelial crosstalk with a focus on disease-relevant inflammatory processes, we used mass spectrometry and characterized the secretome of end stage fibrotic-ILD lung fibroblasts in comparison to non-chronic lung disease (CLD) patient fibroblasts. Out of the over 2000 proteins detected by this experimental approach, 47 proteins were differentially abundant comparing fibrotic-ILD and non-CLD fibroblast secretome. The fibrotic-ILD secretome profile was dominated by chemokines, including CXCL1, CXCL3, and CXCL8, interfering with growth factor signaling orchestrated by Interleukin 11 (IL11), steering fibrogenic cell-cell communication, and proteins regulating extracellular matrix remodeling including epithelial-to-mesenchymal transition. When in turn treating alveolar organoids with IL11, we recapitulated the co-culture results obtained with primary fibrotic-ILD fibroblasts including changes in metabolic activity.

Conclusion: We identified mediators likely contributing to the disease-perpetuating mesenchymal-to-epithelial crosstalk in ILD. In our alveolar organoid co-cultures, we were able to highlight the importance of fibroblast-initiated aberrant epithelial differentiation and confirmed IL11 as a key player in fibrotic-ILD pathogenesis by unbiased fibroblast secretome analysis.

KEYWORDS

cytokine, *IL11*, secretome, interstitial lung disease, organoids, human pluripotent stem cells, disease modeling, co-culture model

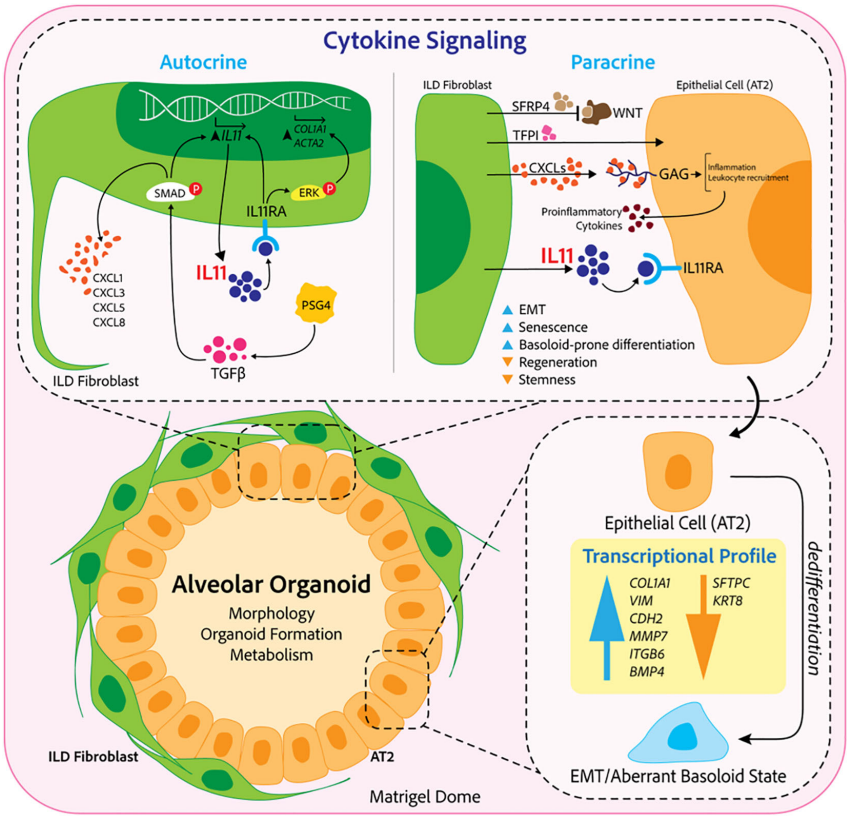

GRAPHICAL ABSTRACT

1 Introduction

Interstitial lung diseases (ILDs) comprise a variety of chronic pulmonary conditions that are characterized by structural remodeling of the gas exchange area (1). ILD pathophysiology is centered on sustained inflammation and progressive scarring, ultimately resulting in irreversible tissue destruction and organ failure. Despite the exact pathogenesis of ILD still being unclear, genetic predisposition, age, sex and environmental exposure are known drivers of the disease (2, 3).

In ILD pathogenesis, fibroblast activation occurs through the impact of exogenous stimuli side-by-side with their activation through innate immune cells, especially monocytes and neutrophils, communicating *via* growth factor signaling and cytokine secretion. Subsequently, lactic acid release from fibroblasts as well as epithelial cells, induced by matrix metalloproteinases (MMPs), fibroblast growth factors and metabolic changes in turn further enhances fibroblast activation and accumulation (4). As a result, fibroblasts become the main loci of extracellular matrix (ECM) production and deposition. Induced by repeated inflammatory epithelial injury that leads to further leucocyte attraction and infiltration of the airspace and further perpetuating the pro-fibrotic circle of events, activated fibroblasts are discussed to induce epithelial-to-mesenchymal transition (EMT) in alveolar epithelial cells *via* SMAD and MAPK signaling (5), (6).

Driving and upholding the outlined pathophysiologic processes in ILD that ultimately result in severe tissue destruction and loss of the alveolar epithelium in end-stage ILD, a tightly knit crosstalk between the activated fibroblast and the damaged epithelium has been proposed (7–9). Here, the role of pathologic growth factor signaling and secreted cytokines such as *transforming growth factor ß (TGF-β)* and *Interleukin 17 (IL17)* were highlighted.

Adding to their detrimental role, activated fibroblasts – next to their capacity for pro-fibrotic signaling and EMT induction – have been shown to alter repair and regeneration of the injured gas-exchange area by affecting alveolar epithelial type 2 stem cell potential (10).

To address apparent knowledge gaps in the cytokine-driven, disease-relevant mesenchymal-to-epithelial crosstalk, we used lung organoids derived from human induced pluripotent stem cells (hiPSCs) through chemical directed differentiation into a sophisticated co-culture model. hiPSC-derived alveolar type 2 cells (iAT2s) are recognized as a useful tool to study lung diseases and regeneration capacities, and are recently emerging as a novel tool in environmental and occupational hazard assessment (11, 12). iAT2-derived alveolar organoids recapitulate the characteristic three-dimensional (3D) structure of alveoli and are thereby ideal to mimic important functions of the gas exchange area *in vitro*. Their potential to study pulmonary disease *in vitro* (13, 14) is particularly versatile when targeting underlying molecular mechanisms (3).

By the integration of this sophisticated methodology in a novel co-culture model, we were able to investigate the impact of primary lung fibroblasts from ILD patients, in our study referring to cases of pulmonary fibrosis, on critical functions of hiPSC-derived alveolar organoids. The combination of this approach with unbiased secretome analysis allowed us to delineate functionally relevant signals of the pathologic crosstalk from the lung mesenchyme towards the alveolar epithelium with the aim to identify potential therapeutic targets.

2 Material and methods

2.1 Human induced pluripotent stem cells (hiPSCs) and directed differentiation into lung progenitors

The hiPSC line BU3NGST was kindly provided by Prof. Darrell Kotton, Boston University, Center for Regenerative Medicine. This cell line is a dual-reporter construct composed of fluorochrome-encoding cassettes targeted to the endogenous NKX2.1 and SFTPC loci (BU3 $NKX2.1^{GFP}$; $SFTPC^{tdTomato}$) (15). hiPSCs were maintained in mTeSR1 (StemCell Technologies), on Matrigel (Corning) coated cell culture plates at 37°C/5% CO_2 in a cell culture CO_2 incubator. Cells were subcultured by using ReLeSR (StemCell Technologies) or Gentle Cell Dissociation Reagent (StemCell Technologies) (16, 17).

BU3NGSTs were differentiated into $NKX2.1^+$ lung progenitor cells and iAT2s as described previously by Jacob et al. (16, 17). In short, hiPSCs were checked for their pluripotency *via* Alkaline Phosphatase staining (ES Cell Characterization Kit, CHEMICON International) or immunofluorescence staining of TRA 181 and SSEA 4 (ES cell characterization Kit, CHEMICON International). Induction of definitive endoderm was conducted *via* STEMdiff Definitive Endoderm Kit, (StemCell Technologies). On day 14 of differentiation, lung progenitor specification was evaluated by immunofluorescence staining of NKX2.1 (Invitrogen) and Albumin (ALB, R&D Systems). $NKX2.1^{GFP+}$ lung progenitor cells were enriched by GFP signal for NKX2.1 based on a previously described protocol. The sorting was performed by FACS cell sorting at MACSQuant Tyto Cell Sorter (Miltenyi Biotec). For data evaluation FlowJo Version 7.2.1 and v10 was used. Purified lung progenitors were seeded in Matrigel (Corning) domes at a cell density of 50 cells/µL and passaged every second week. To increase $SFTPC^{tdTomato+}$ cells CHIR withdrawal and addback was performed. At day 45 of differentiation, iAT2s were enriched by flow cytometry (MACSQuant Tyto Cell Sorter, Miltenyi Biotec) using tdTomato signal for SFTPC expression and subsequently cultured as 3D alveolar organoids. Differentiated $SFTPC^{tdTomato+}$ iAT2s in 3D Matrigel were grown in CK+DCI medium, with media changes every 48 – 72 h. Alveolar organoids were passaged every 14 days.

2.2 Primary human fibroblast culture

Primary human lung fibroblasts from ILD patients, in our study referring to cases of pulmonary fibrosis,and non-CLD (P4) for co-culture experiments (ILD fibroblasts) and MS based secretome

analysis (ILD and non-CLD fibroblasts) were isolated according to a published protocol (18) and obtained through the CPC-M bioArchive at the Comprehensive Pneumology Center in Munich, Germany.

All patients underwent surgery at the LMU Hospital and the Asklepios Pulmonary Hospital Munich-Gauting. Tissue from ILD patients (n = 3, Table 1) was provided through lung transplantation. Control fibroblasts were derived from lung tissue resections of age-matched non-CLD patients (female n = 1, = 3, male n = 2).

The study was approved by the local ethics committee of the Ludwig-Maximilians University of Munich, Germany (Ethic vote #333-10) and written informed consent form was obtained for all study participants.

Human fetal lung fibroblasts (IMR-90, P8) for control co-cultures were obtained from ATCC (Catalog # CCL-186^{TM}) and grown in Dulbecco's Modified Eagle Medium: Nutrient F-12 (DMEM/F12; Gibco) with 20% fetal bovine serum (FBS SUPERIOR, Sigma) and 1% penicillin-streptomycin (Pen Strep, Gibco).

Cells were seeded in 6-well plates. at a density of 1x10^5 cells in 2 mL media (DMEM/F12, 20% FBS, 1% penicillin/streptomycin) per well until reaching 80% confluency. Once confluent, each well was washed three times with a 15-minute incubation per wash with 1 mL of FBS-free culturing medium (DMEM/F12, 1% penicillin/streptomycin) to eliminate remaining FBS. Fibroblasts were cultured for 48 h in FBS-free medium, supernatants were collected and stored at -80°C for further analysis.

2.3 Secretome analysis by mass spectrometry

2.3.1 Sample preparation for proteomics

Each 500 µL supernatant was subjected to tryptic digest applying a modified filter aided sample preparation procedure (19, 20). After protein reduction and alkylation using DTT and iodoacetamide, samples were denatured in UA buffer (8 M urea in 0.1 M Tris/HCl pH 8.5) and centrifuged on a 30 kDa cut-off filter device (PALL or Sartorius) and washed thrice with UA buffer and twice with 50 mM ammoniumbicarbonate (ABC). Proteins were proteolysed for 2 h at room temperature using 0.5 µg Lys-C (Wako) and subsequently for 16 h at 37°C using 1 µg trypsin (Promega). Peptides were collected by centrifugation and acidified with 0.5% trifluoroacetic acid.

2.3.2 Mass spectrometric measurements

LC-MSMS analysis was performed on a Q-Exactive HF mass spectrometer (Thermo Scientific) each online coupled to a nano-RSLC (Ultimate 3000 RSLC; Dionex). For subsequent analysis on the Q-Exactive HF, tryptic peptides were accumulated on a nano trap column (300 µm inner diameter × 5 mm, packed with Acclaim PepMap100 C18, 5 µm, 100 Å; LC Packings) and then separated by reversed phase chromatography (nanoEase MZ HSS T3 Column, 100 Å, 1.8 µm, 75 µm X 250 mm; Waters) in a 80 minutes non-linear gradient from 3 to 40% acetonitrile in 0.1% formic acid at a flow rate of 250 nL/min. Eluted peptides were analyzed by the Q-Exactive HF mass spectrometer equipped with a PepSep PSS1 source. Full scan MS spectra (from m/z 300 to 1500) and MSMS fragment spectra were acquired in the Orbitrap with a resolution of 60.000 or 15.000 respectively, with maximum injection times of 50 ms each. The up to ten most intense ions were selected for HCD fragmentation depending on signal intensity (TOP10 method). Target peptides already selected for MS/MS were dynamically excluded for 30 seconds. Data are available *via* ProteomeXchange with identifier PXD039554 (21, 22).

2.3.3 Protein identification and label-free quantification

Proteome Discoverer 2.5 software (Thermo Fisher Scientific; version 2.5.0.400) was used for peptide and protein identification *via* a database search (Sequest HT search engine, SequestHT score:1) against Swissprot human database (Release 2020_02, 20432 sequences), considering full tryptic specificity, allowing for up to two missed tryptic cleavage sites, precursor mass tolerance 10 ppm, fragment mass tolerance 0.02 Da. Carbamidomethylation of Cys was set as a static modification. Dynamic modifications included deamidation of Asn, Gln and Arg, oxidation of Pro and Met; and a combination of Met loss with acetylation on protein N-terminus. Percolator was used for validating peptide spectrum matches and peptides, accepting only the top-scoring hit for each spectrum, and satisfying the cutoff values for false discovery rate (FDR) < 5%, and posterior error probability < 0.01.

The quantification of proteins was based on abundance values for unique peptides. Abundance values were normalized on total peptide amount and protein abundances were calculated summing up the abundance values for admissible peptides. The final protein ratio was calculated using median abundance values. The statistical significance of the ratio change was ascertained employing the T-test approach

TABLE 1 Patient characteristics.

Patient	Diagnosis	Age at sample collection (years)	Sex	Surgery	Smoking history
1	Connective Tissue Disease related ILD	48	F	Lung transplantation (single)	no
2	Idiopathic pulmonary fibrosis	62	M	Lung transplantation (single)	no
3	Hypersensitivity Pneumonitis, Rheumatoid arthritis	57	F	Lung transplantation	no

described in 23 (23), which is based on the presumption that we look for expression changes for proteins that are just a few in comparison to the number of total proteins being quantified. The quantification variability of the non-changing "background" proteins can be used to infer which proteins change their expression in a statistically significant manner. Proteins with increased or decreased abundance were filtered with the following criteria: proteins were considered to be decreased in abundance below an abundance of ratio of 0.5 fold and increased abundance above 2 fold, proteins identified with a single peptide were excluded and just significant proteins were considered (P value < 0.05, P values were adjusted for multiple testing by Benjamini-Hochberg correction). Additionally, at least two MSMS identifications had to be identified to include the protein ratio.

2.3.4 Enrichment analysis

Pathway enrichment analyses were performed in Cytoscape (3.9.0) with the ClueGo plugin (v2.5.8) for significantly increased or decreased proteins. The following ontologies were used: KEGG (8093), GO_MolecularFunction-EBI-UniProt (18336), GO_BiologicalProcess-EBI-UniProt (18058). Accession IDs were used as identifiers and the analysis was performed with the standard software settings provided in the ClueGo app (24).

2.4 Mesenchymal-epithelial co-culture

Primary lung ILD fibroblasts and IMR-90 (control fibroblast cell line) were grown in cell culture flasks until 70% confluency. A single cell suspension was prepared using 0.25% EDTA-Trypsin (Gibco). iAT2s were grown into alveolar organoids for up to two weeks in Matrigel domes. Single cell suspension was obtained with Dispase (Corning) and 0.25% EDTA-Trypsin as described by Jacob et al. (17). Human ILD and IMR-90 fibroblasts as well as iAT2s were counted and directly seeded either in equal 1:1 (F_{low}) or 1:5 (F_{high}) iAT2s to fibroblasts seeding densities in undiluted Matrigel domes in 8-chamber wells (20 µL Drops, Falcon), 96-well plates (50 µL Drops, Greiner) or 12-well plates (50 µL Drops, Greiner). Co-cultures used CK+DCI media that was changed every 48 h to 72 h for up to 12 days of cultivation.

2.5 Immunofluorescence microscopy

3D alveolar organoids mono- and co-cultures as described in section 2.1 (mono-culture) and 2.4 (co-culture) were cultured in 8-chamber wells for immunofluorescence analysis (Nunc Lab-Tek Chamber Slide System, 8-well, Permanox slide, 0.8 cm^2/well). After alveolar organoids were formed, fixation was achieved with ice cold methanol and acetone (1:1v/v) for 5 minutes at -20°C. Cells were washed with PBS and stained with the respective primary antibody in buffer containing 0.1% BSA and 0.1% Triton X-100 overnight at 4°C. The next day, cells were washed 3 times with PBS and incubated in buffer with the respective fluorescent conjugated secondary antibody at a dilution of 1:500 and DAPI diluted 1:1.000 overnight at 4°C. The following day, cells were washed gently, growth camber removed and remaining microscope slide mounted with fluorescent mounting media (Dako) and covered with a coverslip. Slides were stored at 4°C until imaging. Imaging was performed using a confocal laser scanning microscope (CLSM) Zeiss LSM 880 with Airyscan and edited afterwards using ZEN 2.5 software (Zeiss). Detailed information on the primary and secondary antibodies are given in Supplementary Table 1.

2.6 Operetta high content imaging and Napari organoid counter

Live imaging of all alveolar organoid mono- and co-cultures was performed using the Operetta CLS high-content analysis system (Operetta CLS, PerkinElmer) at time points 5, 8 and 12 days during the co-culture experimental set-up. Pictures were analyzed by the Harmony 3.5.2 high-content imaging and analysis software with PhenoLOGIC.

Multi-plane confocal 3D images were visualized in Napari image viewer (Python) as maximum intensity projections and the automatic measurements obtained from the "Napari organoid counter" (25) were visually checked and manually curated, resulting in output of size and numbers of formed alveolar organoids between iAT2s and human fibroblasts (ILD and control IMR-90). The Canny Edge Detection (26) algorithm is used for identifying the organoids, while pre- and post-processing steps have been included, to ensure the image matches the detector's expected input and the number of detected organoids along with their size is returned. More specifically, the organoids are approximated to ellipses and the algorithm fits orthogonal bounding boxes around each, with the height and width of each box corresponding to the two diameters of the organoid which are then in turn used to approximate the object's area.Quantitative real-time PCR

Co-cultures were lysed in RLT Plus Lysis Buffer (Qiagen) and RNA isolation was performed with the RNeasy Mini Kit (Qiagen) according to the manufacturer's instructions. Cell lysis from organoids and co-culture assays was performed with peqGOLD TriFast (VWR Life Science) as recommended by the manufactures followed by RNA isolation with the RNeasy Mini Kit (Qiagen). RNA was transcribed into cDNA by reverse transcriptase using the High-Capacity cDNA Reverse Transcription Kit (Thermo Fisher Scientific) according to the manufacturer's instructions. 5 ng of cDNA was added to a final concentration volume of 10 µL, Random Nonamers (Metabion) and master mix (Invitrogen, Thermo Fisher Scientific) was added to each RNA sample. cDNA was diluted with ultrapure H_2O. qPCR was performed in 96-well format using the quantitative real-time PCR System (Roche 480 LightCycler). 2 µL cDNA were added to a final reaction volume of 10 µL containing H_2O, 480 SYBR Green (LightCycler, Roche Diagnostics) and the primer mix (100 µM). Gene expression was normalized to *ß-Actin* control for genes *Vimentin* (*VIM*), *Integrin Subunit Beta 6* (*ITGB6*) and *Cadherin 2* (*CDH2*), and normalized to an average of *ß-Actin* and *HRPT* control for genes *Surfactant Protein C* (*SFTPC*), *Keratin 8* (*KRT8*), *Collagen 1A1* (*Col1A1*), *Matrix Metallopeptidase* (*MMP7*) and *Bone*

Morphogenic Protein 4 (*BMP4*), the fold change was calculated using the 2^ (-ddC) method. Sequence information of used primers are given in Supplementary Table 2. Data obtained from qPCR are presented relative to respective control co-cultures, to demonstrate influence of disease background.

2.7 Metabolic activity estimated by WST-1 assay

WST-1 assays were performed at day 2, 3, 5 and 7 of alveolar organoid co-cultures (human ILD or IMR-90 control fibroblasts). WST-1 reagent (Roche Diagnostics) was added to the culture medium in a 1:10 dilution. The culture medium was used as background control. After 2 h of incubation at 37°C and 5% CO_2, 100 µL of media from every sample was transferred to a microplate (Thermo Scientific; Fisher Scientific) and the absorbance of the sample against the background was measured with a TECAN reader (TECAN; infinite M200 PRO).

3 Results

3.1 Fibroblast induced changes in organoid formation and metabolic activity in co-cultured alveolar organoids

An overview of the experimental workflow is provided in Supplementary Figures 1A–C. iAT2s (Figure 1A) were successfully co-cultured with both ILD, in our study referring to cases of pulmonary fibrosis, or IMR-90 control fibroblasts, resulting in the formation of proliferative alveolar organoids (Figure 1B). Cell-cell contact of iAT2s and fibroblasts in (ILD) co-culture was demonstrated by partial encapsulation of alveolar organoids by α-SMA expressing fibroblasts (Figure 1C, white arrows).

Image analysis of the 3D co-cultures revealed a reduction in organoid formation capacity in the presence of human fibroblasts (Figure 1D). Although alveolar organoid size was not significantly affected by fibroblast co-culture (Figures 1B, E), quantitative assessment of organoid size (area, μm^2) and number of images obtained from alveolar organoids and co-cultures with either ILD or IMR-90 control fibroblasts in 1:1 ($F_{ILD/Control\ low}$) or 1:5 ($F_{ILD/Control\ high}$) seeding density (Figures 1B, D) demonstrated a negative correlation of fibroblast seeding density (ILD or IMR-90) with the alveolar organoid formation capacity.

In contrast, co-culture with ILD fibroblasts significantly increased metabolic activity of alveolar organoid in comparison to IMR-90 control co-cultures (Figure 1F).

3.2 Presence of ILD fibroblasts leads to aberrant epithelial gene expression changes

In order to relate the observed changes in organoid formation capacity and metabolic activity (Figure 1) to changes in gene expression, we measured critical markers of stem cell function and epithelial differentiation in co-cultured organoids.

Indicating changes in (stem) cell function and epithelial injury, we showed decreased expression of the alveolar stem cell marker *SFTPC* in the presence of ILD fibroblasts in both seeding ratios (F_{low} and F_{high}; Figure 2A). In line with this, *Keratin 8* (*KRT8*) expression levels were reduced under the impact of ILD primary fibroblasts (Figure 2A). Further, the distal epithelial marker *Integrin Subunit Beta 6* (*ITGB6*) as well as *Bone Morphogenetic Protein 4* (*BMP4*) showed increased transcription in ILD co-cultures when high seeding densities were applied (Figure 2A). Genes associated with regulation of extracellular matrix formation and remodeling including *Collagen 1A1* (*Col1A1*), *N-Cadherin 2* (*CDH2*) and *Vimentin* (*VIM*) showed increased expression in alveolar organoids co-cultured with ILD fibroblasts in high seeding ratios (Figure 2B). Likewise, expression levels of *Matrix Metallopeptidase 7* (*MMP7*) were increased in ILD co-cultures compared to control co-cultures. (Figure 2B).

3.3 ILD fibroblast secretome reveals proinflammatory signaling converging on *IL11* stimulating epithelial remodeling

To characterize fibroblast driven communication resulting in gene expression and phenotypical changes in the alveolar epithelium in ILD, supernatants of ILD and non-CLD fibroblasts were subjected to mass spectrometry (MSMS).

MS analysis detected an overall of 2625 expressed proteins, of which 47 were significantly more and 55 significantly less abundant when comparing ILD-derived fibroblast to non-CLD controls (Supplementary Table 3, 4, Figure 3A). The top 15 differentially expressed proteins (increased and decreased abundance) are listed in Supplementary Tables 1, 2.

Proteins with increased abundance predominantly belonged to the C-X-C motif chemokine family (*CXCL1, CXCL3*, and *CXCL8*), as well as to the interleukin family (*IL13RA, IL11*) and included gap junction proteins (*connexin 43*, *GJA1*). Further, *Pregnancy Specific Beta-1-Glycoprotein 4 (PSG4)* as well as WNT signaling modulator *SFRP4* were found amongst the top 15 proteins.

Accordingly, pathway enrichment analysis of proteins with increased abundance classified the responses as cytokine activity, chemokine-mediated signaling pathway and TNF-signaling pathway. Furthermore, cellular/response to chemokines, *IL17* signaling pathways and neutrophil chemotaxis were identified, indicative of a strong inflammatory response.

ClueGo, a Cytoscape plug-in for network analysis, highlighted proteins associated with rheumatoid arthritis, a disease often complicated by the development of lung fibrosis and characterized by the presence of inflammatory chemokines (Figure 3B).

Proteins with decreased abundance in the in ILD secretome were dominated by candidates involved in ECM production, ECM assembly or ECM reorganization as well as coordination of myofibroblast differentiation (*PDGFRL*) together with a downregulation of proteins involved in complement and coagulation cascade pathways (Figure 3C).

10.3389/fimmu.2023.1128239

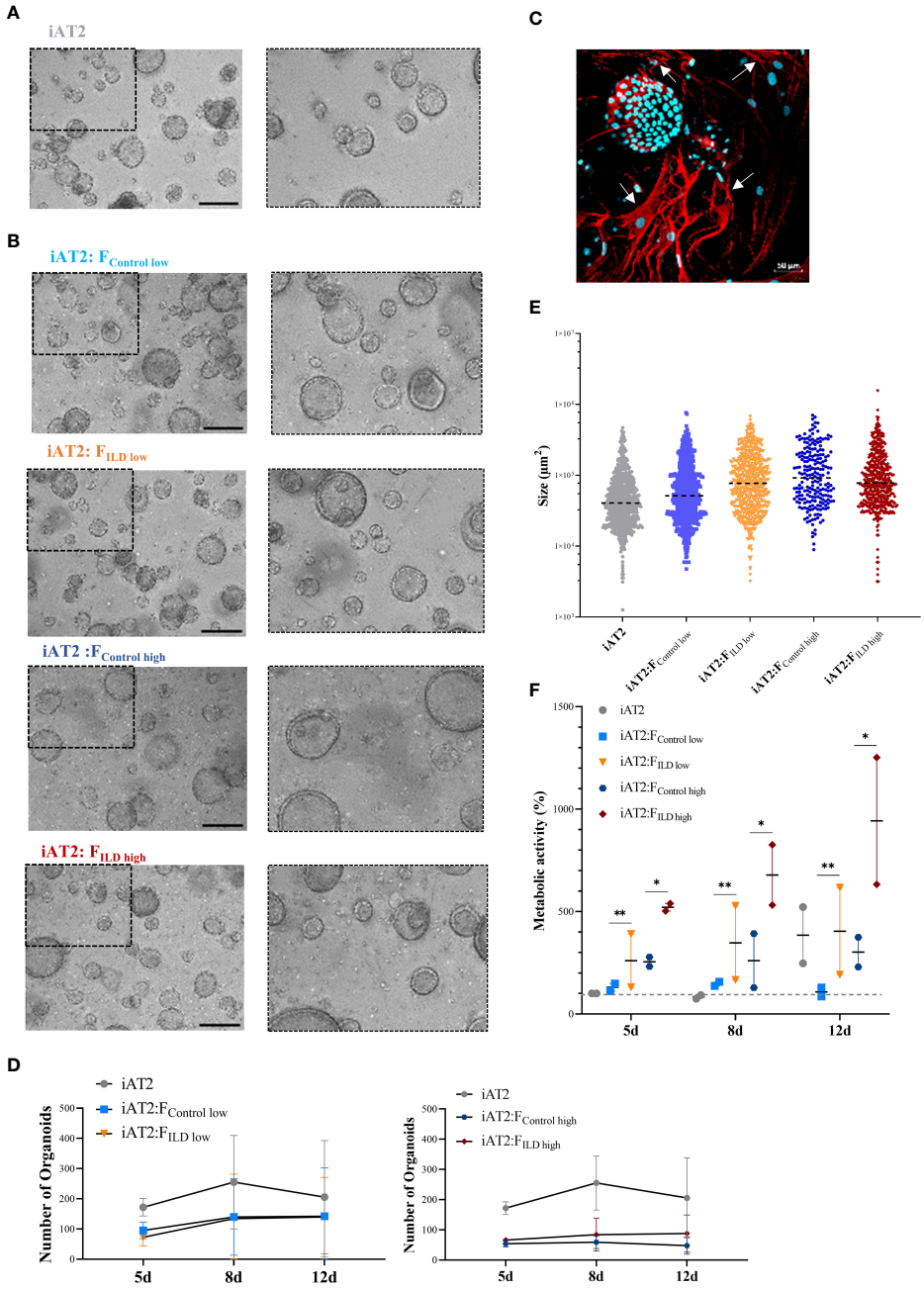

FIGURE 1
(A) Representative maximum intensity projections from high-content images of iAT2s growing as alveolar organoids at day 12. Scale bar 500µm. **(B)** Immunofluorescence of 3D co-culture of iAT2s with ILD fibroblasts at day 12 (α-SMA: red, DAPI: cyan). Scale bar 50 µm. **(C)** Representative maximum intensity projections from high-content images of different co-culture conditions showing iAT2s growing with human fibroblasts for 12 days. Scale bar 500 µm. Zoom-ins show a 3x optical magnification. **(D)** Scatter plots (dashed black lines: median) indicate size (µm2) of organoids in co-cultures at day 12 across three independent biological replicates. **(E)** Number of formed organoids in co-cultures at day 12, N = 3. **(F)** Metabolic activity of co-cultured organoids at 5, 8 and 12 days of co-culture. Results show the increase in percentage across two biological replicates in comparison to d5 iAT2 organoids alone, representing the baseline of 100% metabolic activity (dashed grey line across dataset). Statistics: unpaired t-Test, *p<0.05, **p<0.01.

3.4 *IL11* acts as a driver for aberrant signatures in hiPSC-derived alveolospheres

Based on the MSMS secretome analysis, *IL11* emerged as a top player in the mesenchymal-to-epithelial disease crosstalk. In consequence, we exposed alveolar organoids (Figure 4A) to *IL11* in order to investigate its functional relevance. Experiments ($Dose_{low}$ = 0.5 ng/mL, $Dose_{high}$ = 5 ng/mL) (Figures 4B–D) recapitulated the results observed in epithelial-fibroblasts co-cultures (section 3.1), *i.e.*, we demonstrated reduced organoid formation capacity (Figures 4Biii, C) and increased metabolic activity (WST-1) in *IL11* treated alveolar organoids (treatment

10.3389/fimmu.2023.1128239

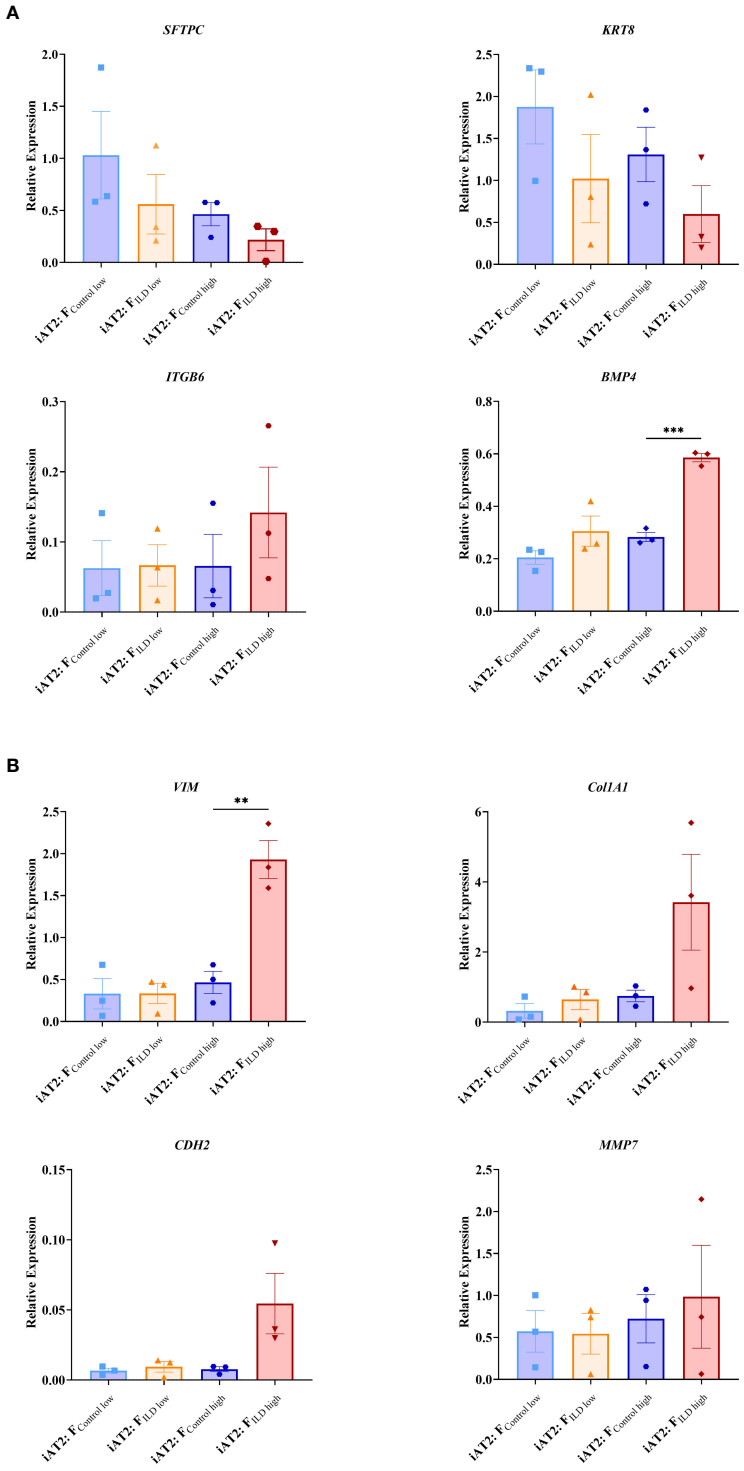

FIGURE 2
Relative gene expression at day 12 measured in AT2s co-cultures with ILD or IMR90 control fibroblasts in two seeding densities (high or low) compared to reference gene expression (HK; average of ß-Actin *(ACTB)* and hypoxanthine guanine phosphoribosyl transferase (*HRPT)*). **(A)** Epithelial and stem cell markers and **(B)** Genes associated with aberrant differentiation of epithelium. N = 3, unpaired t-Test, **p<0.005, ***p<0.0005.

from day 7 - 14 of culture) (Figure 4D). In addition, treatment of growing alveolar organoid monocultures with *IL11* (20 ng/mL) led to an increase in alveolar organoid size followed by apoptosis within 5 days of culture.

4 Discussion

In ILD, sustained inflammation and scarring of the gas exchange area ultimately result in destruction of the pulmonary

10.3389/fimmu.2023.1128239

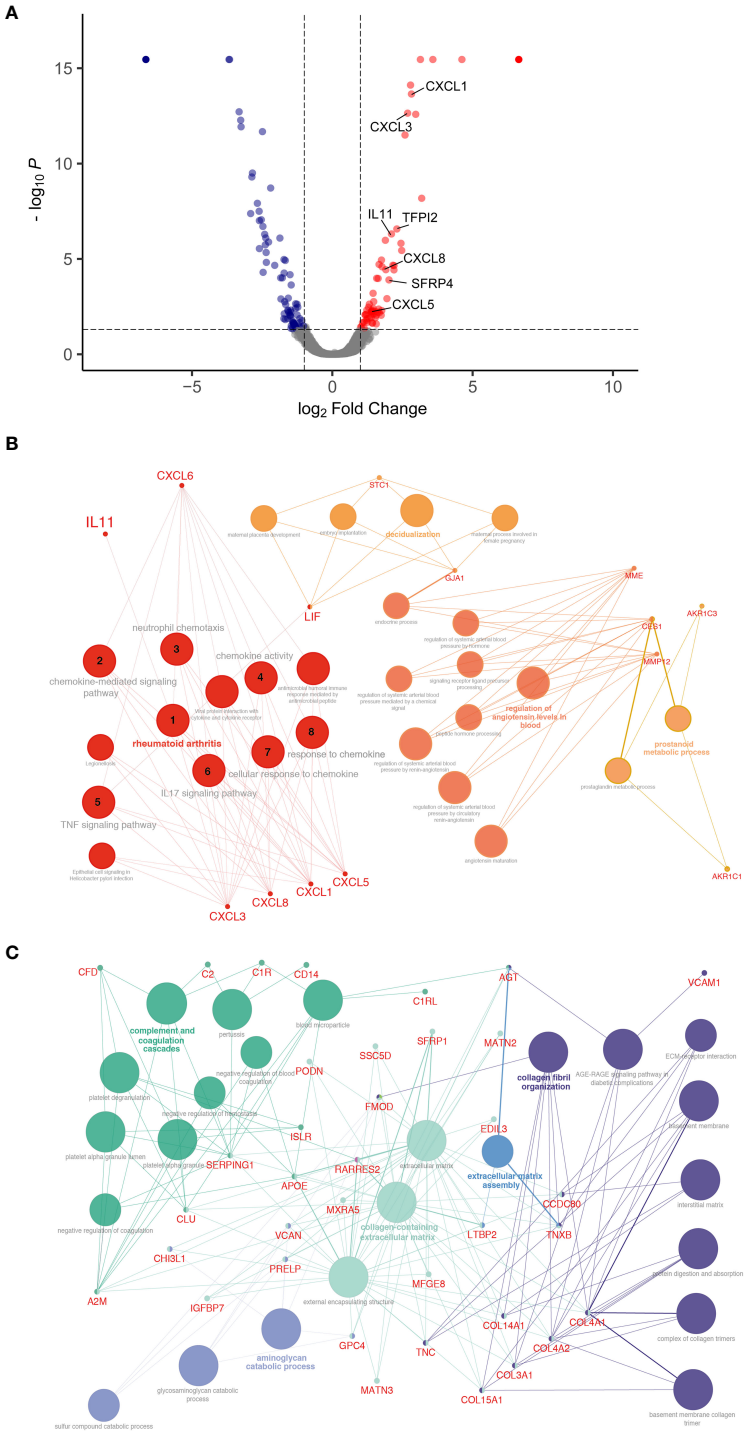

FIGURE 3
Differential protein expression comparing ILD fibroblasts (F_{ILD}) vs. non-chronic lung disease fibroblasts ($F_{control}$). **(A)** Volcano plot visualizing significantly regulated proteins (47 up, 55 down) detected by MS secretome analysis of ILD or non-CLD control fibroblasts. Data showing log_2 fold change against the adjusted P value [log10]. Significantly upregulated proteins are depicted in red and significantly downregulated proteins in blue. (Total: 102 significantly regulated proteins with 5% FDR < 0.05, adj. p_value < 0.05). Pathway enrichment and protein interaction network of proteins with **(B)** increased and **(C)** decreased abundance using the Cytoscape plugin ClueGo. The following ontologies were used: KEGG, molecular functions and biological processes. The connectivity of the pathways is described by functional nodes and edges that are shared between proteins with a kappa score of 0.4. Only enriched pathways are visualized and the node size indicates the p-value (p-value ≤ 0.05). Proteins from the same pathway share the same node color and the bold fonts indicate the most important functional pathways that define the names of each group. Enriched Pathways: 1. rheumatoid arthritis, 2. chemokine-mediated signaling pathway, 3. neutrophil chemotaxis, 4. chemokine activity, 5. *TNF* signaling pathway, 6. *IL17* signaling pathway, 7. cellular response to chemokine, 8. response to chemokine.

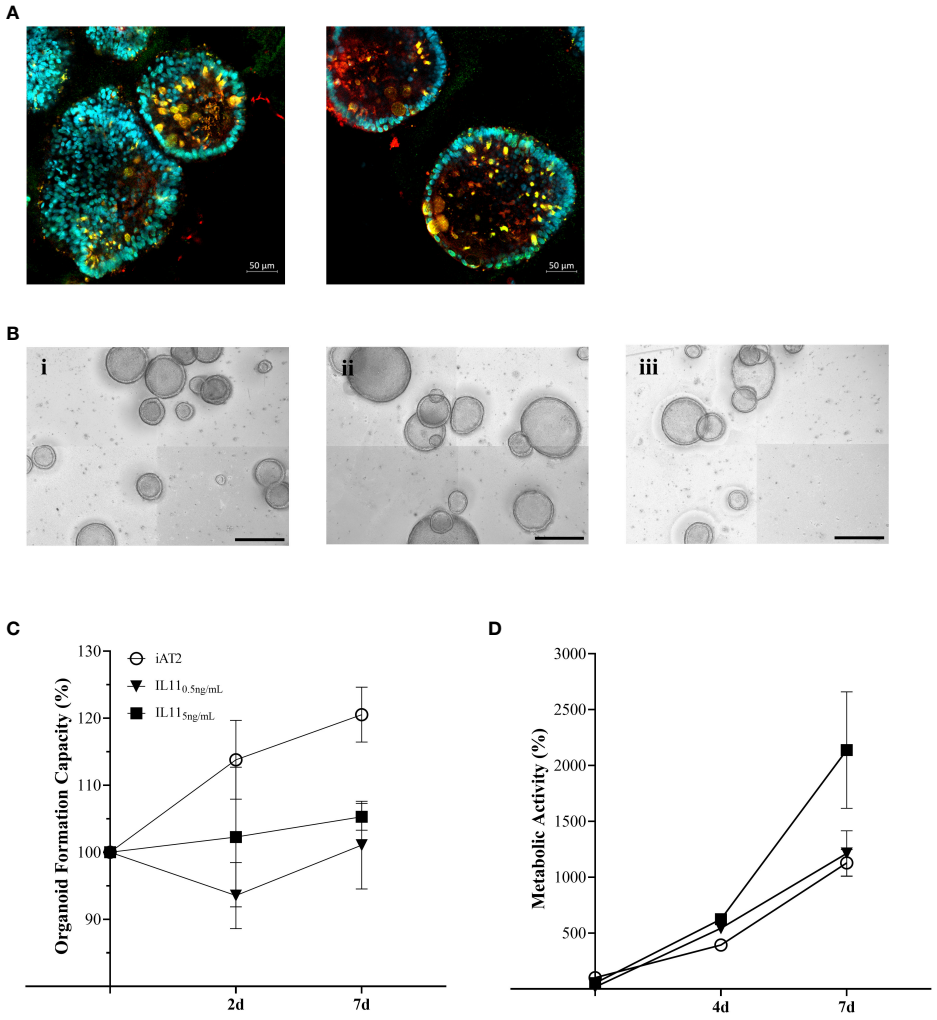

FIGURE 4
(A) Immunofluorescence of untreated alveolar organoids at day 14 of culture (*SFTPC*: red, *NKX2.1*: green, DAPI: cyan). **(B)** Representative maximum intensity projections from high-content images of (i) untreated alveolar organoids, (ii) 0.5 ng/mL or (iii) 5 ng/mL *IL11* treatment. Treatment started at day 7 of culture every 48h. Scale bar, 500 µm. **(C)** Organoid formation capacity of alveolar organoids treated with 0.5 or 5ng/mL *IL11*. **(D)** Metabolic activity of alveolar organoids treated with 0.5 or 5ng/mL *IL11*. **(C, D)** Each value is graphed as percentage of the respective starting culture at day 7 set to 100%.

scaffold and organ failure. Excessive deposition of ECM as well as epithelial damage and dedifferentiation is widely transmitted by the misguided interaction of fibroblasts and epithelial cells (27). Therefore, improved understanding of the mesenchymal-to-epithelial crosstalk remains a centerpiece in finding new avenues to monitor and treat ILD. However, signaling factors with functional relevance and their distinct role in ILD pathogenesis remain understudied.

This study aimed at deciphering disease-relevant candidates of mesenchymal-to-epithelial crosstalk that could serve as potential targets for future therapeutic strategies. By advancing a sensitive human iPSC-derived alveolar organoid culture into a human fibroblast co-culture model, we successfully demonstrated the importance of fibroblast-driven, cytokine-centered signaling in inducing the impairment of key epithelial cell functions, including differentiation and metabolism. In combination with an unbiased proteomic approach, we were able to identify important mediators that translate these effects such as *IL11*, one of the top 15 proteins with increased abundance in ILD, in our study referring to cases of pulmonary fibrosis. The previously identified role of *IL11* in chronic inflammatory lung diseases in line with its potential to drive pro-fibrotic mesenchymal-epithelial crosstalk, supported the relevance of our approach on the one hand, while we were able to contribute the important functional consequences of its signaling in our human alveolar organoid model on the other (7, 8, 28).

In our *in vitro* co-culture approach, primary human pulmonary fibroblasts and iAT2s formed alveolar organoids that successfully recapitulated tissue characteristics of the distal lung in three dimensions, in contrast to 2D, plastic culture conditions (Figure 1). Primary human fibroblasts, both ILD-derived and IMR-90 control cells, demonstrated effects that correlated with seeding density leading to reduced organoid number and increased organoid size after 12 days of co-culture. The findings indicate that the co-culture with fibroblasts per se is able to change

the microenvironment of iAT2s, thereby impacting organoid formation. As studies indicated, that the activation of primary lung fibroblasts in a disease-comparable fashion is easily achieved (29), our findings likely explain the disease-independent fibroblast effects in alveolar organoids.

In contrast, the significant increase in metabolic activity was provoked by diseased human fibroblasts in high-seeding ratios, indicating their potential to impact on the metabolic program of the epithelial cell, potentially indicating epithelial dedifferentiation or EMT (30–32). These considerations are supported by the expression signature characterizing the co-cultures: The decrease in *SFTPC* expression (33–36) we observed in the ILD co-cultures points towards the loss of epithelial stem cell characteristics, as *SFTPC* expression is sensitive to epithelial inflammation and injury, lately supported by studies in Sars-CoV-2 infected alveolar organoids (10). Differentiation of AT2s is key for regeneration in injured alveoli marked by their expression of transient basaloid features such as *Keratin 5* (*KRT5*) and the amount of alveolar *KRT5*$^{+}$ basaloid cells directly correlates with disease progression in pulmonary fibrosis (29, 37, 38), mirrored by the decreased expression observed in our study. Closely related, downregulation of *KRT8*, an important marker of AT2 to (pre)AT1 transdifferentiation during epithelial regeneration (38, 39) was associated with the increased expression of EMT markers in a murine bleomycin lung injury model including pro-fibrogenic proteins such as *ITGB6* (39). In line with these findings, we demonstrated increased *ITGB6* expression in ILD co-cultures. Its release from the plasma membrane potentially reflects the activation of EMT-like processes in lung organoids, accompanied by the decrease of expressed *KRT8*. Further supporting these findings, we showed the elevated expression of *BMP4* and *MMP7*, critical regulators of EMT in pulmonary fibrosis (40), in lung organoids co-cultured with ILD fibroblasts. *MMP7* has furthermore been highlighted for its function as a plasma biomarker in idiopathic pulmonary fibrosis (33, 41), in line with its detection in our study.

Co-culture of alveolar organoids with ILD fibroblasts also specifically changed the expression of genes involved in ECM biosynthesis including the increased transcription of *Col1A1*, *VIM* and *CDH2*, well-known players in fibrotic lung disease (33, 34) (38), as compared to organoid monocultures. Linking back to the indications of aberrant basal transdifferentiation in fibroblast co-culture discussed above (29), the basaloid cells show increased ECM protein expression, next to their increase in *BMP4* and *ITGB6* expression, again successfully detected in our model.

We next were able to provide deeper insight into the relevant mediators of mesenchymal-to-epithelial crosstalk related to the observed changes in organoid phenotype by screening the supernatant of ILD or control fibroblasts using mass spectrometry (42). Cytokines that belong to the C-X-C motif family dominated the protein signature in the secretome, demonstrating their increased abundance in ILD. These signaling molecules act on the *CXCR1* and *CXCR2* receptor, as well as regulate the expression of cytokines from the interleukin family, central to the pathogenesis of fibrotic and inflammatory lung diseases such as IPF and acute respiratory distress syndrome (3, 8, 36, 43). The majority of the differentially abundant proteins are proinflammatory cytokines that primarily act on neutrophil, monocyte or lymphocyte recruitment (*CXCL1, CXCL3, CXCL5, CXCL8*). The proinflammatory response is complemented by the regulation of proteins that play a role in cellular senescence and activation of *TGF-ß* such as the Pregnancy-Specific Glycoprotein (PSG) family, *PSG 4, 5, 6* or in the induction of a hypercoagulable tissue state (*TFPI2*). Other important proteins such as *SFRP4* directly inhibit WNT signaling, thereby modulating cell growth and differentiation, particularly of AT2s to AT1s (44). *WNT* serum levels are discussed as biomarkers for lung fibrosis and EMT. *WNT* modulation and *TGF-ß* solubilization in particular could account for the change in organoid number and size and support our observations in gene expression levels that indicate epithelial transdifferentiation into aberrant basaloid cells or EMT in the presence of ILD fibroblasts.

IL11, centrally orchestrating the ILD protein profile as observed by pathway enrichment, was identified among the top 15 candidates in the ILD fibroblast secretome. *IL11* is known to be expressed in pro-inflammatory fibroblasts extracted from IPF lungs. The cytokine belongs to the *IL6* family and is induced by *TGF-ß* and other proinflammatory mediators [*IL1β, IL17, IL22*, reactive oxygen species (ROS)]. It can either activate fibroblasts to differentiate into myofibroblasts in an autocrine fashion through ERK/SMAD canonical signaling, which results in pro-fibrotic protein expression (*COL1A1, ACTA2*), or it stimulates epithelial cells (paracrine loop) through activating *ERK* signaling cascades, thereby inducing cellular senescence, EMT, cellular dysfunction and impaired regeneration (8). Results from our co-culture model indicate both autocrine and paracrine signaling of *IL11* as we demonstrated indication of EMT, stem cell dysfunction as well as ECM production, i.e., upregulation of collagen expression in line with 8 (8). Similar to the results obtained from ILD fibroblast co-culture in different seeding densities, *IL11* treatment of alveolar organoid monocultures resulted in a dose dependent increase in metabolic activity, elevated expression of mesenchymal markers and decreased AT2 stemness and identity. Dose-dependent, *IL11* even induced apoptotic cell death, in line with its role in senescence and stem cell function observed in alveolar organoids (36). Similarly, *IL11* alone induced fibrotic changes in healthy alveolar organoids whereas knock-out of *IL11* expression in diseased organoids reversed organoid fibrosis in a model of the Hermansky-Pudlak syndrome-associated interstitial pneumonia, a disease with high similarity to IPF (3). Supporting our co-culture findings in this regard, *IL11* exposure impacts on AT2 progenitor function, thereby likely suppressing the formation of mature AT2s as described by Kortekaas and colleagues (35, 36).

Taken together, our results strongly support the central role of *IL11* signaling as the cytokine holds the potential to strongly influence the intricate crosstalk between the (then activated (myo)) fibroblasts and the injured epithelium, central in the progression of fibrosis in ILD. We successfully demonstrated the potential of our lung organoid co-culture model derived from hiPSCs and primary fibroblasts to display critical consequences of the malfunctional crosstalk such as aberrant dedifferentiation and basaloid-prone signatures (33, 45). In this context, *IL11* likely holds an important role in misguided alveolar function, differentiation

and thereby regeneration, important functions as a potential therapeutic target to regain alveolar crosstalk homeostasis (46).

Data availability statement

The datasets presented in this study can be found in online repositories. The names of the repository/repositories and accession number(s) can be found in the article. The mass spectrometry proteomics data presented in the study have been deposited to the ProteomeXchange Consortium via the PRIDE partner repository with the dataset identifier PXD039554..

Ethics statement

The studies involving human participants were reviewed and approved by Ludwig-Maximilians University of Munich, Germany. (Ethic vote #333-10). The patients/participants provided their written informed consent to participate in this study.

Author contributions

MK, AH and CV conceived and planned the experiments. MK, EG-R, PC and EMG carried out the main experiments. FS and SA contributed to sample preparation. A-CK and SH performed the mass spectrometry analysis. LH performed additional data analysis and figure composition. CB, GB, MP and ML conceived, discussed and developed the AI based organoid counter. RAH headed patient sample retrieval and documentation and contributed clinical background to the study. MK, CV, TS, A-CK, SH, JB and AH contributed substantially to the interpretation of the results. MK and CV took the lead in writing the manuscript. All authors provided critical feedback and helped shape the research, analysis and drafting of the manuscript.

Funding

This project was supported by the Research Training Group GRK2338 of the DFG, LMU Munich. Further funding was received by the German Center of Lung Research (DZL) and Helmholtz Munich.

Acknowledgments

We gratefully acknowledge the provision of human biomaterial (primary human fibroblasts) and clinical data from the CPC-M bioArchive and its partners at the Asklepios Biobank Gauting, the LMU Hospital and the Ludwig-Maximilians-Universität München. We thank the patients and their families for their support. We wish to thank the Kotton Lab especially Prof. Darrell Kotton by providing the hiPSC cell line. We are grateful to David Kutschke (LHI, Helmholtz Center Munich) for technical assistance. We thank Dr. Kenji Schorpp and Dr. Kamyar Hadian (Research Unit Signaling and Translation, Molecular Targets and Therapeutics Center, Helmholtz Zentrum München, Germany) for their excellent support with the Operetta System. We thank the Research Unit Analytical Pathology (AAP, Helmholtz Center Munich) with Dr. Ulrike Buchholz and Dr. Annette Feuchtinger for their assistance during confocal imaging. We thank Benoite Champon and Dr. Minodora Brimpari for their help with the cell sorting at the MACSQuant Tyto Cell Sorter. We thank Zeynep Ertüz for creating the graphical abstract. Graphics were created with BioRender.com. The manuscript has been published as a preprint on Biorxiv under (47).

Conflict of interest

The authors declare that the research was conducted in the absence of any commercial or financial relationships that could be construed as a potential conflict of interest.

Publisher's note

All claims expressed in this article are solely those of the authors and do not necessarily represent those of their affiliated organizations, or those of the publisher, the editors and the reviewers. Any product that may be evaluated in this article, or claim that may be made by its manufacturer, is not guaranteed or endorsed by the publisher.

Supplementary material

The Supplementary Material for this article can be found online at: https://www.frontiersin.org/articles/10.3389/fimmu.2023.1128239/full#supplementary-material

References

1. Glasser SW, Hardie WD, Hagood JS. Pathogenesis of interstitial lung disease in children and adults. *Pediatr Allergy Immunol Pulmonol* (2010) 23(1):9–14. doi: 10.1089/ped.2010.0004

2. Lederer DJ, Martinez FJ. Idiopathic pulmonary fibrosis. *N Engl J Med* (2018) 378 (19):1811–23. doi: 10.1056/NEJMra1705751

3. Strikoudis A, Cieślak A, Loffredo L, Chen YW, Patel N, Saqi A, et al. Modeling of fibrotic lung disease using 3D organoids derived from human pluripotent stem cells. *Cell Rep* (2019) 27(12):3709–3723.e3705. doi: 10.1016/j.celrep.2019.05.077

4. Dwyer AR, Ellies LG, Holme AL, Pixley FJ. A three-dimensional co-culture system to investigate macrophage-dependent tumor cell invasion. *J Biol Methods* (2016) 3(3):e49. doi: 10.14440/jbm.2016.132

5. Kim KK, Sheppard D, Chapman HA. TGF-β1 signaling and tissue fibrosis. *Cold Spring Harb Perspect Biol* (2018) 10(4):a022293. doi: 10.1101/cshperspect.a022293

6. O'Dwyer DN, Ashley SL, Moore BB. Influences of innate immunity, autophagy, and fibroblast activation in the pathogenesis of lung fibrosis. *Am J Physiology-Lung Cell Mol Physiol* (2016) 311(3):L590–601. doi: 10.1152/ajplung.00221.2016

7. Ng B, Dong J, D'Agostino G, Viswanathan S, Widjaja AA, Lim WW, et al. Interleukin-11 is a therapeutic target in idiopathic pulmonary fibrosis. *Sci Transl Med* (2019) 11(511):eaaw1237. doi: 10.1126/scitranslmed.aaw1237

8. Ng B, Cook SA, Schafer S. Interleukin-11 signaling underlies fibrosis, parenchymal dysfunction, and chronic inflammation of the airway. *Exp Mol Med* (2020) 52(12):1871–8. doi: 10.1038/s12276-020-00531-5

9. Yao L, Zhou Y, Li J, Wickens L, Conforti F, Rattu A, et al. Bidirectional epithelial-mesenchymal crosstalk provides self-sustaining profibrotic signals in pulmonary fibrosis. *J Biol Chem* (2021) 297(3):101096. doi: 10.1016/j.jbc.2021.101096

10. Mou H. Induced pluripotent stem cell-derived alveolar type II heterogeneity: Revealed by SFTPC expression. *Am J Respir Cell Mol Biol* (2021) 65(4):345–6. doi: 10.1165/rcmb.2021-0242ED

11. Kong J, Wen S, Cao W, Yue P, Xu X, Zhang Y, et al. Lung organoids, useful tools for investigating epithelial repair after lung injury. *Stem Cell Res Ther* (2021) 12(1):95. doi: 10.1186/s13287-021-02172-5

12. Kastlmeier MT, Guenther EM, Stoeger T, Voss C. Lung organoids for hazard assessment of nanomaterials. *Int J Mol Sci* (2022) 23(24):15666. doi: 10.3390/ijms232415666

13. Nikolić MZ, Sun D, Rawlins EL. Human lung development: recent progress and new challenges. *Development* (2018) 145(16):dev163485. doi: 10.1242/dev.163485

14. Nikolić MZ, Hogan MZN. Lung stem cells in development, health and disease. In: *ERS monograph* (2021). doi: 10.1183/2312508X.erm9121

15. Hawkins F, Kramer P, Jacob A, Driver I, Thomas DC, McCauley KB, et al. Prospective isolation of NKX2-1-expressing human lung progenitors derived from pluripotent stem cells. *J Clin Invest* (2017) 127(6):2277–94. doi: 10.1172/jci89950

16. Jacob A, Morley M, Hawkins F, McCauley KB, Jean JC, Heins H, et al. Differentiation of human pluripotent stem cells into functional lung alveolar epithelial cells. *Cell Stem Cell* (2017) 21(4):472–488.e410. doi: 10.1016/j.stem.2017.08.014

17. Jacob A, Vedaie M, Roberts DA, Thomas DC, Villacorta-Martin C, Alysandratos K-D, et al. Derivation of self-renewing lung alveolar epithelial type II cells from human pluripotent stem cells. *Nat Protoc* (2019) 14(12):3303–32. doi: 10.1038/s41596-019-0220-0

18. Heinzelmann K, Lehmann M, Gerckens M, Noskovičová N, Frankenberger M, Lindner M, et al. Cell-surface phenotyping identifies CD36 and CD97 as novel markers of fibroblast quiescence in lung fibrosis. *Am J Physiol Lung Cell Mol Physiol* (2018) 315 (5):L682–l696. doi: 10.1152/ajplung.00439.2017

19. Wiśniewski JR, Zougman A, Nagaraj N, Mann M. Universal sample preparation method for proteome analysis. *Nat Methods* (2009) 6(5):359–62. doi: 10.1038/nmeth.1322

20. Grosche A, Hauser A, Lepper MF, Mayo R, von Toerne C, Merl-Pham J, et al. The proteome of native adult müller glial cells from murine retina. *Mol Cell Proteomics* (2016) 15(2):462–80. doi: 10.1074/mcp.M115.052183

21. Deutsch EW, Bandeira N, Sharma V, Perez-Riverol Y, Carver JJ, Kundu DJ, et al. The ProteomeXchange consortium in 2020: enabling 'big data' approaches in proteomics. *Nucleic Acids Res* (2019) 48(D1):D1145–52. doi: 10.1093/nar/gkz984

22. Perez-Riverol Y, Bai J, Bandla C, García-Seisdedos D, Hewapathirana S, Kamatchinathan S, et al. The PRIDE database resources in 2022: a hub for mass spectrometry-based proteomics evidences. *Nucleic Acids Res* (2021) 50(D1):D543–52. doi: 10.1093/nar/gkab1038

23. Navarro P, Trevisan-Herraz M, Bonzon-Kulichenko E, Núñez E, Martínez-Acedo P, Pérez-Hernández D, et al. General statistical framework for quantitative proteomics by stable isotope labeling. *J Proteome Res* (2014) 13(3):1234–47. doi: 10.1021/pr4006958

24. Bindea G, Mlecnik B, Hackl H, Charoentong P, Tosolini M, Kirilovsky A, et al. ClueGO: a cytoscape plug-in to decipher functionally grouped gene ontology and pathway annotation networks. *Bioinformatics* (2009) 25(8):1091–3. doi: 10.1093/bioinformatics/btp101

25. Bukas C. *HelmholtzAI-Consultants-Munich/napari-organoid-counter: Latest versions of dependencies (v0.1.1)*. Zenodo (2022). doi: 10.5281/zenodo.7065206

26. Canny J. (1986). "A computational approach to edge detection," in: *IEEE Transactions on Pattern Analysis and Machine Intelligence*, Vol. PAMI-8. pp. 679–98. doi: 10.1109/TPAMI.1986.4767851

27. Lewis KJR, Hall JK, Kiyotake EA, Christensen T, Balasubramaniam V, Anseth KS. Epithelial-mesenchymal crosstalk influences cellular behavior in a 3D alveolus-fibroblast model system. *Biomaterials*. (2018) 115:124–34. doi: 10.1016/j.biomaterials.2017.11.008

28. Cook SA, Schafer S. Hiding in plain sight: Interleukin-11 emerges as a master regulator of fibrosis, tissue integrity, and stromal inflammation. *Annu Rev Med* (2020) 71:263–76. doi: 10.1146/annurev-med-041818-011649

29. Kathiriya JJ, Wang C, Zhou M, Brumwell A, Cassandras M, Le Saux CJ, et al. Human alveolar type 2 epithelium transdifferentiates into metaplastic KRT5+ basal cells. *Nat Cell Biol* (2022) 24(1):10–23. doi: 10.1038/s41556-021-00809-4

30. Kalluri R. EMT: When epithelial cells decide to become mesenchymal-like cells. *J Clin Invest* (2009) 119(6):1417–9. doi: 10.1172/JCI39675

31. Kalluri R, Weinberg RA. The basics of epithelial-mesenchymal transition. *J Clin Invest* (2009) 119(6):1420–8. doi: 10.1172/JCI39104

32. Wang Y, Dong C, Zhou BP. Metabolic reprogram associated with epithelial-mesenchymal transition in tumor progression and metastasis. *Genes Dis* (2020) 7 (2):172–84. doi: 10.1016/j.gendis.2019.09.012

33. Adams TS, Schupp JC, Poli S, Ayaub EA, Neumark N, Ahangari F, et al. Single-cell RNA-seq reveals ectopic and aberrant lung-resident cell populations in idiopathic pulmonary fibrosis. *Sci Adv* (2020) 6(28):eaba1983. doi: 10.1126/sciadv.aba1983

34. Katzen J, Beers MF. Contributions of alveolar epithelial cell quality control to pulmonary fibrosis. *J Clin Invest* (2020) 130(10):5088–99. doi: 10.1172/JCI139519

35. Kortekaas RK, Burgess JK, Webster M, Gosens R. IL11 negatively impacts adult lung alveolar organoid formation. *ERJ Open Res* (2021) 7(suppl 6):81. doi: 10.1183/23120541.Lsc-2021.81

36. Kortekaas R, Geillinger-Kästle K, Borghuis T, Belharch K, Webster M, Timens W, et al. IL-11 disrupts alveolar epithelial progenitor function. *bioRxiv* (2022). doi: 10.1101/2022.11.11.516088

37. Khan P, Roux J, Blumer S, Knudsen L, Jonigk D, Kuehnel MP, et al. Alveolar basal cells differentiate towards secretory epithelial- and aberrant basaloid-like cells *In vitro*. *Cells* (2022) 11(11):1820. doi: 10.3390/cells11111820

38. Ng B, Huang KY, Pua CJ, Lim W-W, Kuthubudeen F, Hii AA, et al. Interleukin-11 causes alveolar type 2 cell dysfunction and prevents alveolar regeneration. *bioRxiv* (2022). doi: 10.1101/2022.11.11.516109

39. Strunz M, Simon LM, Ansari M, Kathiriya JJ, Angelidis I, Mayr CH, et al. Alveolar regeneration through a Krt8+ transitional stem cell state that persists in human lung fibrosis. *Nat Commun* (2020) 11(1):3559. doi: 10.1038/s41467-020-17358-3

40. Molloy EL, Adams A, Moore JB, Masterson JC, Madrigal-Estebas L, Mahon BP, et al. BMP4 induces an epithelial-mesenchymal transition-like response in adult airway epithelial cells. *Growth Factors* (2008) 26(1):12–22. doi: 10.1080/08977190801987166

41. Bauer Y, White ES, de Bernard S, Cornelisse P, Leconte I, Morganti A, et al. MMP-7 is a predictive biomarker of disease progression in patients with idiopathic pulmonary fibrosis. *ERJ Open Res* (2017) 3(1):00074-2016. doi: 10.1183/23120541.00074-2016

42. Strieter RM, Gomperts BN, Keane MP. The role of CXC chemokines in pulmonary fibrosis. *J Clin Invest* (2007) 117(3):549–56. doi: 10.1172/jci30562

43. Mukaida N. Pathophysiological roles of interleukin-8/CXCL8 in pulmonary diseases. *Am J Physiology-Lung Cell Mol Physiol* (2003) 284(4):L566–77. doi: 10.1152/ajplung.00233.2002

44. Abdelwahab EMM, Rapp J, Feller D, Csongei V, Pal S, Bartis D, et al. Wnt signaling regulates trans-differentiation of stem cell like type 2 alveolar epithelial cells to type 1 epithelial cells. *Respir Res* (2019) 20(1):204. doi: 10.1186/s12931-019-1176-x

45. Habermann AC, Gutierrez AJ, Bui LT, Yahn SL, Winters NI, Calvi CL, et al. Single-cell RNA sequencing reveals profibrotic roles of distinct epithelial and mesenchymal lineages in pulmonary fibrosis. *Sci Adv* (2020) 6(28):eaba1972. doi: 10.1126/sciadv.aba1972

46. Lin CR, Bahmed K, Kosmider B. Impaired alveolar re-epithelialization in pulmonary emphysema. *Cells* (2022) 11(13):2055. doi: 10.3390/cells11132055

47. Kastlmeier MT, Rodriguez EG, Cabanis P, Guenther EM, König A-C, Han L, et al. Cytokine signaling converging on IL11 in ILD fibroblasts provokes aberrant epithelial differentiation signatures. *bioRxiv* (2022). doi: 10.1101/2022.12.20.521114